Fixed-time Distributed Voltage and Reactive Power Compensation of Islanded Microgrids Using Sliding-mode and Multi-agent Consensus Design

Mohamed Ghazzali, Mohamed Haloua, and Fouad Giri

***Abstract*—This paper investigates a fixed-time distributed voltage and reactive power compensation of islanded microgrids using sliding-mode and multi-agent consensus design. A distributed sliding-mode control protocol is proposed to ensure voltage regulation and reference tracking before the desired preset fixed-time despite the unknown disturbances. Accurate reactive power sharings among distributed generators are maintained. The secondary controller is synthesized without the knowledge of any parameter of the microgrid. It is implemented using a sparse one-way communication network modeled as a directed graph. A comparative simulation study is conducted to highlight the performance of the proposed control strategy in comparison with finite-time and asymptotic control systems with load power variations.**

***Index Terms*—Secondary controller, microgrids, reactive power control, voltage control.**

I. Introduction

MICROGRIDS are small-scale electrical distribution networks, consisting of distributed power sources, loads and energy storage systems. Primary control of microgrids maintains the stability of frequency and voltage, which causes the magnitudes of frequency and voltage to deviate from their nominal values. Emerged as a natural control system for microgrids, distributed secondary control restores the frequency and the voltage to their nominal operation points and achieves accurate power sharing in both grid-connected and islanded operation modes.

Distributed secondary control has been widely discussed in literature [1]-[11]. Several techniques including proportional-integral (PI) control [9], feedback control [3]-[6], [10]-[12], adaptive control [6], [13] and model predictive control (MPC) [14], [15] among others are developed to address secondary control objectives of microgrids, which are voltage control, frequency control and power sharing. However, many shortcomings are to be addressed. In [9], a distributed PI controller is proposed for secondary control of voltage and frequency. Only small signal stability is guaranteed which means that large external disturbances, i.e., load variations during peak hours and the connection or disconnection of a power source, can destabilize the power system and cause voltage or frequency to swell or sag. In [5], [6], [10]-[12], feedback linearization and variants of feedback control are used to achieve secondary control of microgrids. However, a nonlinear model of AC microgrids is used in the design of the distributed control protocols that require detailed parameters of the microgrid. Practically, load parameters and transmission line impedances among other parameters are unknown and time-variant, which is challenging to apply the controllers in real applications. Adaptive control is suggested in [6], [13] for secondary control of AC microgrids. A major drawback of this approach is high computation complexity of the control law. In fact, in the adaptation technique, the control gains are updated in real time via a complicated and time-consuming mathematical approach as linear matrix inequalities (LMIs) or differential equation systems in [6] and neural networks in [13]. Thus, a control hardware with high computation capacity is required, which increases the implementation cost of the control system. In the case of neural network based adaptive control, a prior learning phase of the neurons based on experimental data is required for the design of the controller, which complicates the design, tuning and implementation of the controller. In [14], [15], the model of predictive secondary controllers is proposed for AC microgrids. The MPC approach is based on the model, which indicates that a model of the microgrid is required to calculate the output of the controller. Consequently, its robustness will depend on the accuracy of the model, which makes the controller vulnerable to modeling uncertainties. In addition, a fully detailed model of the microgrid can not be used in the design procedure as some parameters are practically unknown or difficult to obtain, which means that the unmodeled dynamics of the microgrid will always hinder the performance of the controller.

Furthermore, the distributed secondary controllers can be categorized into asymptotic controllers [2], [5]-[10] and finite-time controllers [1], [3], [4]. In asymptotic control, the

Manuscript received: May 9, 2019; revised: September 9, 2019; accepted: March 5, 2020. Date of CrossCheck: March 5, 2020. Date of online publication: November 26, 2020.

This work was supported by Morocco's National Center for Scientific and Technical Research within the Research Excellence Scholarships Program.

M. Ghazzali (corresponding author) and M. Haloua are with the Electrical Engineering Department, Mohammadia School of Engineers, University Mohammed V, Rabat, Morocco (e-mail: ghazzalimohamed1@gmail.com; haloua@emi.ac.ma).

F. Giri is with the Caen Automation Laboratory (LAC), Caen Normandie University (UNICAEN), Caen, France (e-mail: fouad.giri@unicaen.fr).

DOI: 10.35833/MPCE.2019.000308

reference is only a limit of the terminal voltage or frequency of DG when time goes to infinity. Practically, reference tracking and disturbance rejection cannot be achieved in a finite time as the tracking error cannot be canceled using asymptotic control protocols. In finite-time control, the reference is reached in a finite time. The settling-time depends on the uncertain initial conditions of the system. An explicit relation between the parameters of the controller and the settling-time is not always available.

Sliding-mode control (SMC) is widely used to design the control systems and has been applied in the areas including robotics [16]-[19], power converter control [20]-[23], motor control [24]-[27], and power systems [28]-[32]. SMC is designed to achieve reference tracking and regulation despite uncertainties of the parameter and external disturbance, which makes it suitable for applications with unknown dynamics and under uncertain conditions. In power systems, parameter uncertainties and external disturbances are constant issues [33]-[37]. In fact, most of the parameters are time-varying, which makes exact measurement of these parameters a challenging task. The fluctuations of voltage and frequency are caused by the nonlinear nature of loads and their unpredictable power consumption variations. As a result, SMC is suitable for microgrid control as it is robust to the unmodeled dynamics, variated parameters, and unknown disturbances. In addition, SMC has a straightforward design procedure and several variants of SMC have been designed with continuous and discontinuous outputs for several classes of linear and nonlinear systems. Therefore, the sliding-mode approach can be easily applied.

Considering the advantages of SMC and obviating the shortcomings of the secondary microgrid controllers, a fixed-time distributed SMC-based control approach is proposed for the secondary control of AC microgrid. Hence, the voltage regulation and reference tracking before the desired preset fixed-time can be ensured. And the accuracy of reactive power sharing is ensured among distributed generators (DGs) at its nominal levels. These objectives are guaranteed despite the uncertain microgrid parameters and the unknown disturbances. Moreover, the design procedure is model-free since no prior knowledge of load power demand, transmission line impedance or the microgrid topology is required.

The rest of the paper is organized as follows. In Section II, a large-signal dynamic model of islanded microgrids is presented. Section III presents the design of the fixed-time distributed secondary controller with voltage and reactive power sharing. A comparative simulation study on finite-time asymptotic secondary controllers and conventional power sharing protocol with load power variations is presented in Section IV. Finally, Section V concludes the paper.

II. Large-signal Dynamical Model of Islanded Microgrids

An islanded microgrid is adopted with n DGs, where every DG i, $i \in \{1, 2, ..., n\}$ contains a primary energy source connected to a voltage-source converter (VSC), an RL series filter, a step-up transformer (Y-Δ) with transformation ratio m_i, and a shunt capacitor $C_{t,i}$ attenuating the impact of high-frequency voltage harmonics of the local load. Each DG i is connected to a set $N_i \subset \{1, 2, ..., n\}$ of neighboring DGs at the corresponding point of common coupling (PCC) through transmission lines modeled as a RL series circuits. A schematic of two connected DGs is depicted in Fig. 1, where $V_{i,d}^*$ and $V_{i,q}^*$ are the references of the direct and quadratic components of the output voltage of DG i, respectively; $V_{t,i}$, $I_{t,i}$, $R_{t,i}$, $L_{t,i}$ are the voltage, current, resistance, and impetance of VSC terminal, respectively; and the subscript $i+1$ denotes DG $i+1$.

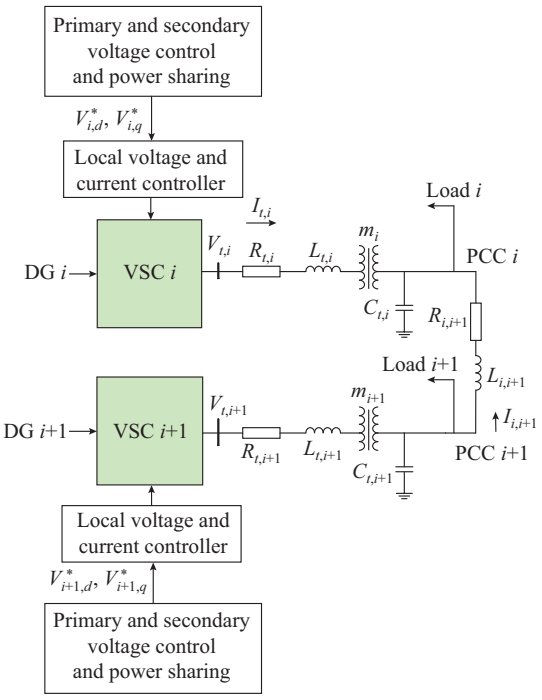

Fig. 1. Schematic of two connected DGs.

DG i can be modeled in the d-q framework by the follwoing large-signal dynamical model [38]:

$$\begin{cases} I_{i,d} = m_i I_{t,i,d} - C_{t,i}\dfrac{\mathrm{d}}{\mathrm{d}t}V_{i,d} + C_{t,i}\omega_n V_{i,q} \\ I_{i,q} = m_i I_{t,i,q} - C_{t,i}\dfrac{\mathrm{d}}{\mathrm{d}t}V_{i,q} - C_{t,i}\omega_n V_{i,d} \\ \dfrac{\mathrm{d}}{\mathrm{d}t}\boldsymbol{x}_i = \boldsymbol{A}_i\boldsymbol{x}_i + \sum\limits_{j\in N_i}\boldsymbol{A}_{ij}\boldsymbol{x}_j + \boldsymbol{B}_i\boldsymbol{u}_i + \boldsymbol{D}_i\boldsymbol{w}_i \\ V_{t,i,d} = V_{t,i,d}^* \\ V_{t,i,q} = V_{t,i,q}^* \\ V_{t,i,d}^* = -\omega_n L_{t,i} I_{t,i,q} + K_{pci}(I_{t,i,d}^* - I_{t,i,d}) + K_{ici}\int(I_{t,i,d}^* - I_{t,i,d})\,\mathrm{d} \\ V_{t,i,q}^* = \omega_n L_{t,i} I_{t,i,d} + K_{pci}(I_{t,i,q}^* - I_{t,i,q}) + K_{ici}\int(I_{t,i,q}^* - I_{t,i,q})\,\mathrm{d} \\ I_{t,i,d}^* = F_i I_{i,d} - \omega_n C_{t,i} V_{i,q} + K_{pvi}(V_{i,d}^* - V_{i,d}) + K_{ivi}\int(V_{i,d}^* - V_{i,d})\,\mathrm{d} \\ I_{t,i,q}^* = F_i I_{i,q} - \omega_n C_{t,i} V_{i,d} + K_{pvi}(V_{i,q}^* - V_{i,q}) + K_{ivi}\int(V_{i,q}^* - V_{i,q})\,\mathrm{d} \end{cases} \tag{1}$$

where $I_{i,d}$ and $I_{i,q}$ are the direct and quadratic components of the output current of DG i, respectively; $V_{i,d}$ and $V_{i,q}$ are the

direct and quadratic components of the output voltage of DG i, respectively, and the output voltage of DG i is also the voltage of PCC i; F_i is the feed-forward coefficent; $V^*_{t,i,d}$ and $V^*_{t,i,q}$ are the references of the direct and quadratic components of the terminal voltage of VSC, respectively, which are calculated by the local voltage and current of VSC controller [39]; $V_{t,i,d}$ and $V_{t,i,q}$ are the direct and quadratic components of VSC terminal voltage, respectively; $I^*_{t,i,d}$ and $I^*_{t,i,q}$ are the references of the direct and quadratic components of the VSC terminal current, respectively; $I_{t,i,d}$ and $I_{t,i,q}$ are the direct and quadratic components of the VSC terminal current, respectively; $I_{L,i,d}$ and $I_{L,i,q}$ are the direct and quadratic components of the current of load i; $\omega_n = 2\pi f_n$ is the nominal pulsation with $f_n = 50$ Hz nominal frequency; $\boldsymbol{A}_i$, $\boldsymbol{A}_{ij}$, $\boldsymbol{B}_i$, and $\boldsymbol{D}_i$ are the state-space matrices [40]; $\boldsymbol{x}_i = [V_{i,d}, V_{i,q}, I_{t,i,d}, I_{t,i,q}]^{\mathrm{T}}$ is the state vector; $\boldsymbol{u}_i = [V_{t,i,d}, V_{t,i,q}]$ is the input; K_{pvi}, K_{ivi}, K_{pci}, and K_{ici} are the control gains of the PI controllers in the internal voltage and current control loops designed for high-frequency disturbance rejection and the filter output damping to avoid any resonance with the external network, respectively [39], which are tuned using the symmetrical optimum tool [41]; and $\boldsymbol{w}_i = [I_{L,i,d}, I_{L,i,q}]$ is the load current consumption considered as a known disturbance and an exogenous input to the system for $i \in \{1, 2, ..., n\}$. With the relatively high switching frequency of VSC, it is safe to neglect the switching artifact via average-value modeling. Since the dynamics of the DC-bus can be safely neglected assuming an ideal source from the DG side [39], we can obtain $V_{t,i,d} = V^*_{t,i,d}$ and $V_{t,i,q} = V^*_{t,i,q}$.

The state-space matrices $\boldsymbol{A}_i$, $\boldsymbol{A}_{ij}$, $\boldsymbol{B}_i$, and $\boldsymbol{D}_i$ are defined as [40]:

$$\boldsymbol{A}_i = \begin{bmatrix} -\dfrac{1}{C_{t,i}} \sum\limits_{j \in N_i} \dfrac{R_{ij}}{Z_{ij}^2} & \omega_i - \dfrac{1}{C_{t,i}} \sum\limits_{j \in N_i} \dfrac{X_{ij}}{Z_{ij}^2} & \dfrac{m_i}{C_{t,i}} & 0 \\ -\omega_i + \dfrac{1}{C_{t,i}} \sum\limits_{j \in N_i} \dfrac{X_{ij}}{Z_{ij}^2} & -\dfrac{1}{C_{t,i}} \sum\limits_{j \in N_i} \dfrac{R_{ij}}{Z_{ij}^2} & 0 & \dfrac{m_i}{C_{t,i}} \\ -\dfrac{R_{t,i}}{L_{t,i}} & 0 & -\dfrac{m_i}{L_{t,i}} & \omega_i \\ 0 & -\dfrac{m_i}{L_{t,i}} & -\omega_i & -\dfrac{R_{t,i}}{L_{t,i}} \end{bmatrix} \tag{2}$$

$$\begin{cases} \boldsymbol{A}_{ij} = \dfrac{1}{C_{t,i}} \begin{bmatrix} \dfrac{R_{ij}}{Z_{ij}^2} & \dfrac{X_{ij}}{Z_{ij}^2} & 0 & 0 \\ -\dfrac{X_{ij}}{Z_{ij}^2} & \dfrac{R_{ij}}{Z_{ij}^2} & 0 & 0 \\ 0 & 0 & 0 & 0 \\ 0 & 0 & 0 & 0 \end{bmatrix} \\ \boldsymbol{B}_i = \begin{bmatrix} 0 & 0 \\ 0 & 0 \\ \dfrac{1}{L_{t,i}} & 0 \\ 0 & \dfrac{1}{L_{t,i}} \end{bmatrix} \end{cases} \tag{3}$$

$$\boldsymbol{D}_i = \begin{bmatrix} -\dfrac{1}{C_{t,i}} & 0 \\ 0 & -\dfrac{1}{C_{t,i}} \\ 0 & 0 \\ 0 & 0 \end{bmatrix} \tag{4}$$

where $\omega_i = 2\pi f_i$ is the output pulsation of DG i and f_i is its output frequency; $Z_{ij} = \sqrt{R_{ij}^2 + \omega_i^2 L_{ij}^2}$ is the transmission line impedance; and $X_{ij} = \omega_i L_{ij}$ is the transmission line reactance.

The output active and reactive power P_i and Q_i can be calculated from the output voltage and current in the d-q frame using:

$$\begin{cases} \dfrac{\mathrm{d}}{\mathrm{d}t} P_i = -f_{ci} P_i + f_{ci} (V_{i,d} I_{i,d} + V_{i,q} I_{i,q}) \\ \dfrac{\mathrm{d}}{\mathrm{d}t} Q_i = -f_{ci} Q_i + f_{ci} (V_{i,q} I_{i,d} - V_{i,d} I_{i,q}) \end{cases} \tag{5}$$

where f_{ci} is the cut-off frequency of the low-pass filters used to extract the fundamental component of P_i and Q_i.

The communication network of the microgrid is described using graphs. Consider a n-order weighted directed graph (digraph) $G = (V, E)$ with $V = (v_1, v_2, ..., v_n)$ set of nodes and $E \subseteq V \times V$ set of directed edges. $\boldsymbol{A}$ weight $a_{ij} \geq 0$ is associated with every edge. $a_{ij} > 0$ if there is an edge from node j to node i. If agent j communicates its state information to agent i, then $a_{ij} = 0$. $\boldsymbol{A} = (a_{ij})_{n \times n}$ is called the adjacency matrix of the graph G. The graph Laplacian matrix of G, $\boldsymbol{L}(G) = \boldsymbol{L}$, is defined as $\boldsymbol{L} = \boldsymbol{D} - \boldsymbol{A}$, where $\boldsymbol{D} = \mathrm{diag}\{d_1, d_2, ..., d_n\}$ and $d_i = \sum\limits_{j=1}^{n} a_{ij}$.

Unlike the existing models of microgrids, the interactions between DGs are considered in the proposed model. It also includes the nonlinearties introduced by the filter, the shunt capacitance, the loads, and the step-up transformers.

III. Fixed-time Distributed Secondary Voltage and Reactive Power Control

The control system developed in this paper is a secondary control strategy with voltage and reactive power sharing in hierarchical control framework. The primary control is given as:

$$\begin{cases} V^*_{i,d} = V_{ind} - D_q Q_i \\ V^*_{i,q} = 0 \end{cases} \tag{6}$$

where V_{ind} and D_q are the secondary control output voltage and reactive power droop coefficient, respectively. DG i generates the desired voltage reference, thus $V^*_{i,d} = V_{i,d}$ and $V^*_{i,q} = V_{i,q}$. Then, (6) can be written as:

$$\begin{cases} V_{i,d} = V_{ind} - D_q Q_i \\ V_{i,q} = 0 \end{cases} \tag{7}$$

Since $V_{qi} = 0$, the output voltage magnitude of DG i $V_{i,mag}$ satisfies $V_{i,mag} = \sqrt{V_{i,d}^2 + V_{i,q}^2}$. Thus, controlling the output voltage magnitude is the same as controlling its direct component.

The primary voltage and reactive power control aligns the output voltage magnitude to the d-axis of the voltage reference.

Secondary voltage control is designed to ensure a good trade-off between the conflicting objectives of voltage regulation and maintain the reactive power sharing accuracy in the same pattern as in the primary control:

$$D_{q1}Q_1 = D_{q2}Q_2 = ... = D_{qn}Q_n = \Delta V_{\max} \tag{8}$$

where $\Delta V_{\max}$ is the maximum allowable voltage deviations.

Differentiating the voltage droop characteristics twice will yield:

$$\frac{\mathrm{d}^2}{\mathrm{d}t^2}V_{ind} = \frac{\mathrm{d}^2}{\mathrm{d}t^2}V_{i,d} + D_q\frac{\mathrm{d}^2}{\mathrm{d}t^2}Q_i = u_{vQi} \tag{9}$$

where u_{vQi} is the auxiliary control input. According to (9), the secondary voltage and reactive power control of islanded microgrids can be transformed to a leader-follower second-order consensus problem for the following linear second-order multi-agent system:

$$\frac{\mathrm{d}^2}{\mathrm{d}t^2}V_{ind} = u_{vQi} \qquad i \in \{1, 2, ..., n\} \tag{10}$$

Definition: the leader-follower second-order consensus in multi-agent systems is presented as:

$$\frac{\mathrm{d}^2}{\mathrm{d}t^2}z_i(t) = v_i(t) \qquad i \in \{1, 2, ..., n\} \tag{11}$$

where z_i is the position of the i^{th} agent; and v_i is the i^{th} agent control input.

Leader-follower second-order consensus in multi-agent system (11) is achieved under any initial conditions and $\forall i \in \{1, 2, ..., n\}$. We can obtain:

$$\begin{cases} \lim\limits_{t \to +\infty} \|z_i(t) - z_0(t)\| = 0 \\ \lim\limits_{t \to +\infty} \left\| \dfrac{\mathrm{d}}{\mathrm{d}t}z_i(t) - \dfrac{\mathrm{d}}{\mathrm{d}t}z_0(t) \right\| = 0 \end{cases} \tag{12}$$

We propose the non-singular terminal sliding-mode auxiliary control law u_{vQi} based on the voltage magnitude and the reactive power information from the neighbors of DG i:

$$u_{vQi} = u_{v_i} + u_{Q_i} \tag{13}$$

$$u_{v_i} = \left(\sum_{j\in N_i} a_{ij} + b_i\right)^{-1}\left(-\gamma_{v_i}\cdot \operatorname{sign}(s_i(e^p_{v_i}, e^v_{v_i})) + \sum_{j\in N_i} a_{ij}u_j - \frac{p_i - 2q_i}{p_i}\left(\left(\frac{\pi p_i}{4T_i^{cs}q_i}\right)^{p_i/(p_i-2q_i)} e_{v_i}^{v\,1-[2q_i/(p_i-2q_i)]}F_{p_i,q_i}(e^p_{v_i}) + \frac{\sqrt{2}\,\xi_v}{2\eta_v T^{cr}}\mu_\tau((e^v_{v_i})^{2q_i/(p_i-2q_i)})(e^v_{v_i})^{-[2q_i/(p_i-2q_i)]}((s_i(e^p_{v_i}, e^v_{v_i}))^{1-(2\eta_v/\xi_v)} + n^{2\eta_v/\xi_v}((s_i(e^p_{v_i}, e^v_{v_i}))^2)^{2\eta_v/\xi_v}(s_i(e^p_{v_i}, e^v_{v_i}))^{1-2\eta_v/\xi_v}\right)\right) \tag{14}$$

$$u_{Q_i} = \left(\sum_{j\in N_i} a_{ij} + b_i\right)^{-1}\left(-\gamma_{Q_i}\cdot \operatorname{sign}(s_i(e^p_{Q_i}, e^v_{Q_i})) + \sum_{j\in N_i} a_{ij}u_j - \frac{p_i - 2q_i}{p_i}\left(\left(\frac{\pi p_i}{4T_i^{cs}q_i}\right)^{p_i/(p_i-2q_i)} e_{Q_i}^{v\,1-[2q_i/(p_i-2q_i)]}F_{p_i,q_i}(e^p_{Q_i}) + \frac{\sqrt{2}\,\xi_q}{2\eta_q T^{cr}}\mu_\tau((e^v_{Q_i})^{2q_i/(p_i-2q_i)})(e^v_{Q_i})^{-(2q_i/(p_i-2q_i))}\left((s_i(e^p_{Q_i}, e^v_{Q_i}))^{1-(2\eta_q/\xi_q)} + n^{2\eta/\xi}((s_i(e^p_{Q_i}, e^v_{Q_i}))^2)^{2\eta_q/\xi_q}(s_i(e^p_{Q_i}, e^v_{Q_i}))^{1-(2\eta_q/\xi_q)}\right)\right) \tag{15}$$

where $e_i^p = \sum_{j\in N_i} a_{ij}(v_i - v_j) + b_i(v_i - v_0)$ and $e_i^v = \sum_{j\in N_i} a_{ij}(\dot{v}_i - \dot{v}_j) + b_i(\dot{v}_i - \dot{v}_0)$ are the voltage tracking errors and the derivative, respectively; $e^p_{Q_i} = \sum_{j\in N_i} a_{ij}(D_{Q_i}Q_i - D_{Q_j}Q_j)$ and $e^v_{Q_i} = \sum_{j\in N_i} a_{ij}(D_{Q_i}\dot{Q}_i - D_{Q_j}\dot{Q}_j)$ are the reactive power sharing errors and the derivative, respectively, and D_{Q_i} and D_{Q_j} are the reactive power droop coefficients; T^{cr} is a time constant; T_i^{cs} is the lowest upper-bound of the sliding-time; $b_i > 0$ is the pinning gain and it is non-zero only for the agents that have access to the reference voltage amplitude v_0; and p_i, q_i, η_v, ξ_v, η_q, ξ_q, γ_{v_i}, and γ_{Q_i} are the control parameters that verifies the following conditions:

$$\begin{cases} 0 < q_i/p_i < 0.25 \\ 0 < \eta_v/\xi_v < 0.5 \\ 0 < \eta_q/\xi_q < 0.5 \\ \gamma_{v_i} > 0 \\ \gamma_{Q_i} > 0 \end{cases} \tag{16}$$

Denote $\boldsymbol{B} = \operatorname{diag}\{b_i\}_{i\in\{1,2,...,n\}}$, and D_{Q_i} is the reactive power droop coefficient. $F_{p_i,q_i}(\cdot)$ and $\mu_\tau(\cdot)$ with $\tau > 0$ are defined as:

$$F_{p_i,q_i}(x) = (\cos h((x^2)^{q_i/p_i}))^{p_i/(p_i-2q_i)} + \frac{2q_ip_i}{p_i(p_i-2q_i)}\cdot (e_i^p)^{2q_i/p_i}\sin h((x^2)^{q_i/p_i})(\cos h((x^2)^{q_i/p_i}))^{2q_i/(p_i-2q_i)} \tag{17}$$

$$\mu_\tau(x) = \begin{cases} \sin\left(\dfrac{\pi x^2}{2\tau^2}\right) & |x| \le \tau \\ 1 & \text{otherwise} \end{cases} \tag{18}$$

$s_i(x, y)$ is the sliding surface defined as:

$$s_i(x, y) = y^{p_i/(p_i-2q_i)} + \frac{\pi p_i}{4T_i^{cs}q_i}x(\cos h((x^2)^{q_i/p_i}))^{p_i/(p_i-2q_i)} \tag{19}$$

Figure 2 shows the block diagram of the distributed fixed-time voltage and reactive power controller.

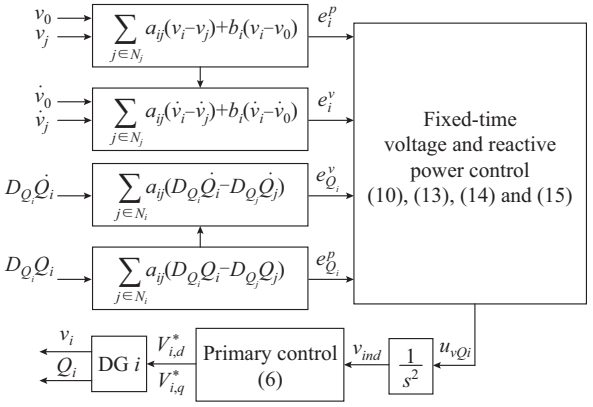

Fig. 2. Block diagram of fixed-time distributed voltage and reactive power controller.

$T^{cr} + 2\tau^{(p_i-2q_i)/(2q_i)}/\gamma_i$ is an upper bound of the reaching time of the secondary SMC of DG i, $i \in \{1, 2, ..., n\}$.

The desired prefixed upper bound of the settling time is expressed as:

$$T = T^{cr} + \max_i (T_i^{cs}) + \max_i \left(\frac{2\tau^{(p_i - 2q_i)/(2q_i)}}{\gamma_i} \right) \tag{20}$$

Theorem: if the control protocol in (15), (16), (17), and (18) is applied, then the fixed-time leader-follower consensus tracking is achieved before the prefixed settling time upper bound (20). Thus, voltage regulation and reference tracking are met in the fixed-time $T_{settling}$ without hindering reactive power sharing, i.e., $T_{settling} \le T$ is verified.

Proof: the result in the Theorem is valid for u_{v_i} and u_{Q_i}, separately [42]. However, to prove that the result is valid for the superposition of the two nonlinear control laws, i. e., $u_{vQi} = u_{v_i} + u_{Q_i}$, we consider the Lyapunov function $V = \sum_{i=1}^{n} (s_i^2(e_{v_i}^p, e_{v_i}^v) + s_i^2(e_{Q_i}^p, e_{Q_i}^v))$. Using $\mu_\tau(x) + \mu_\tau(y) \le \mu_\tau\left((x+y)/2\right)$ with $\mu_\tau\left((x+y)/2\right) = \mu_{\tau/\sqrt{2}}(x+y)$ and $x^a + y^a \le (x+y)^a$, $\forall x, y, a \in R_+^*$, and following similar demonstration steps as in [42], it is concluded that $\lim_{t \to t_r} V = 0$. Then, $\lim_{t \to t_r} s_i(x,y) = 0$, where t_r is the reaching time of the sliding surface $s_i(x,y) = 0$. Then, $t_r < T^{cr} + \max_i \left(2\tau^{(p_i - 2q_i)/(2q_i)} / \gamma_i \right)$ is verified. On the sliding surface, i. e., when $s_i = 0$, if we denote $e_i \in \{e_{v_i}^p, e_{Q_i}^p, e_{v_i}^v, e_{Q_i}^v\}$, the sliding motion dynamics can be described by $\dot{e}_i = -\left(\pi p_i / 4 q_i T_i^{cs}\right) (e_i^p)^{1-(2q/p)} \cos h(((e_i^p)^2)^{q/p})$. Thus we can obtain $2 e_i \dot{e}_i = -\left(\pi p_i / 2 q_i T_i^{cs}\right) (e_i^p)^{2(1-(q/p))} \cos h(((e_i^p)^2)^{q/p})$. By denoting $V_e = e_i^2$, the aforementioned equation can be written as $\frac{q}{p} \frac{V_e^{(q/p)-1} \mathrm{d}V_e}{\cos h(V_e^{q/p})} = -\frac{\pi}{2T_i^{cs}} \mathrm{d}t$, which is equivalent to $\frac{\mathrm{d}V_e^{q/p}}{\cos h(V_e^{q/p})} = \frac{\pi}{2T_i^{cs}} \mathrm{d}t$. Integrating this equation from t_r to t yields $\arcsin(\tan h((e_i^2(t))^{q/p})) = -\pi(t - t_r) / 2T_i^{cs} + \arcsin(\tan h((e_i^2(t_r))^{q/p}))$. At the settling-time t_s of the sliding motion, $e_i = 0$. Thus, $t_s = (2T_i^{cs}/\pi) \arcsin(\tan h((e_i^2(t_r))^{q/p})) \le T_i^{cs}$. The tracking errors $e_{v_i}^p$, $e_{Q_i}^p$, $e_{v_i}^v$, $e_{Q_i}^v$, $i \in \{1, 2, ..., n\}$ converge to zero at $T_{settling}$. Then $T_{settling} \le T^{cr} + \max_i (T_i^{cs}) + \max_i \left(2\tau^{(p_i - 2q_i)/(2q_i)} / \gamma_i \right)$ is verified. Since $v_i - v_0 = (\boldsymbol{L} + \boldsymbol{B}) e_{v_i}^p$, the reference voltage magnitude is reached at $T_{settling}$.

Remark 1: the term $2\tau^{(p_i - 2q_i)/(2q_i)} / \gamma_i$ can be neglected for sufficient high values of γ_i and low values of τ, and $T = T^{cr} + \max_i (T_i^{cs})$ is verified by the upper bound of the prefixed settling time. However, for very small values of $T^{cr} + \max_i (T_i^{cs})$, the effect of the term $2\tau^{(p_i - 2q_i)/(2q_i)} / \gamma_i$ can be reduced but can not be negligible without hindering the controller performance as high values of γ_i increase the chattering effect.

Remark 2: an important feature of the proposed control approach is that the design procedure is straightforward. No knowledge of the microgrid parameter is required. The desired settling-time upper bounds are specified directly in the control law, which makes the tuning process simple. And the only step left is to choose γ_i and τ as explained in Remark 2. In addition, the convergence at the desired settling-time is mathematically guaranteed despite the unknown disturbances.

IV. Comparative Simulation Study

The performance of the proposed fixed-time secondary voltage control is verified with load power variations in comparison with finite-time and asymptotic secondary voltage control. The performance of the proposed protocol of fixed-time reactive power sharing in maintaining power sharing accuracy is compared with the conventional one in [3], [4] and others representing the benchmark for power sharing accuracy, i. e, the nominal level to be maintained within the microgrid. The test system used in the simulations is a low-voltage islanded AC microgrid (nominal frequency $f_0 = \omega_0/(2\pi) = 50$ Hz and nominal voltage magnitude $V_0 = 380$ V) containing four DGs and four loads connected via the communication network. And the network is modeled by the directed graph depicted in Fig. 3. The arrows in the graph indicates the voltage and reactive power data flow direction. DG1 is the leader node, thus the only DG gets access to the reference voltage magnitude with the pinning gain $b_1 = 1$. For the other DGs, $b_i = 0$, $i \in \{2, 3, 4\}$.

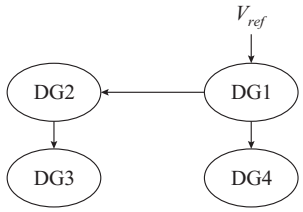

Fig. 3. Topology of microgrid.

Except for the internal voltage and current loop parameters, the DG specifications are adopted from [40]. The filter parameters and the droop coefficients are summarized in Table I. The droop coefficients are assumed so that the voltage deviations are less than the maximum allowable voltage deviation below 10% [43]. Therefore, to achieve high control performance, the maximum allowable voltage deviation is $\Delta V_{\max} = 2\%$. The shunt capacitance $C_t = 62.86$ μH and the transformer ratio $k = 0.6/13.8$ are used for the four DGs. Active and reactive power variations of the loads are presented in Figs. 4 and 5. The control gains of the internal voltage and current loops are tuned as follows: $K_{pv} = K_{pvi} = 150$, $K_{iv} = K_{ivi} = 250$, $K_{pc} = K_{pci} = 100$, and $K_{ic} = K_{ici} = 10$, $\forall i \in \{1, 2, 3, 4\}$.

TABLE I
Microgrid Parameters

DG	Filter parameter		Droop coefficient	
	R_t (mΩ)	L_t (μH)	D_p	D_q
1	1.2	93.7	2.08×10^{-5}	1.210×10^{-3}
2	1.6	94.8	2.10×10^{-5}	1.214×10^{-3}
3	1.5	107.7	2.11×10^{-5}	1.217×10^{-3}
4	1.5	90.6	2.12×10^{-5}	1.218×10^{-3}

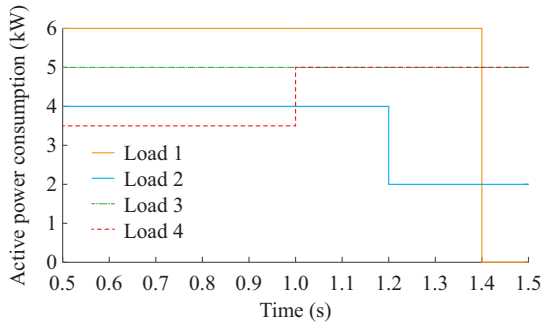

Fig. 4. Active power variation of load.

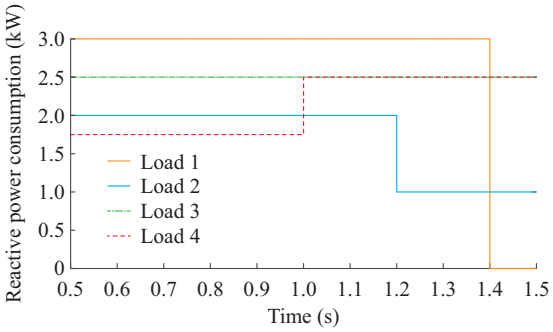

Fig. 5. Reactive power variation of load.

The parameters of voltage and reactive power controllers are set as: $q_i/p_i = 3/37$, $\eta_v/\xi_v = \eta_q/\xi_q = 0.1$, $T^{cr} = 5$ ms and $T_i^{cs} = 5$ ms, $i \in \{1,2,3,4\}$. As $T^{cr} + T_i^{cs}$ is very small, several values of τ and γ_i are tested to reduce the term $2\tau^{(p_i - 2q_i)/(2q_i)}$ without increasing the chattering effect. $\tau = 1 \times 10^{-3}$, $\gamma_{v_i} = 2.4 \times 10^6$, and $\gamma_{Q_i} = 10$ achieve the desired effect and will be used in this paper.

To highlight the efficiency of the proposed fixed-time control, the finite-time and the asymptotic secondary controllers in [4] and [10] have the same settling-time as those of the proposed controller.

The simulations are conducted considering the following scenario.

1) At $t = 0$: the simulation is initialized and the primary control is activated.

2) At $t = 0.8$ s: the proposed secondary control system is applied.

3) At $t = 1$ s: active power and reactive power of load 4 are increased.

4) At $t = 1.2$ s: active power and reactive power of load 2 are decreased.

5) At $t = 1.4$ s: load 1 is disconnected from the microgrid.

The results of the simulations are shown in Figs. 6-8. As shown in Fig. 6, the droop-based primary control maintains the microgrid voltage stability. Accurate power sharing can be shown in Fig. 8, which does not cancel the reference tracking error and maintain the microgrid back to the nominal operation conditions. Thus, the primary control results in a deviation in the voltage amplitude of DGs. As a result, the secondary control is required for voltage restoration.

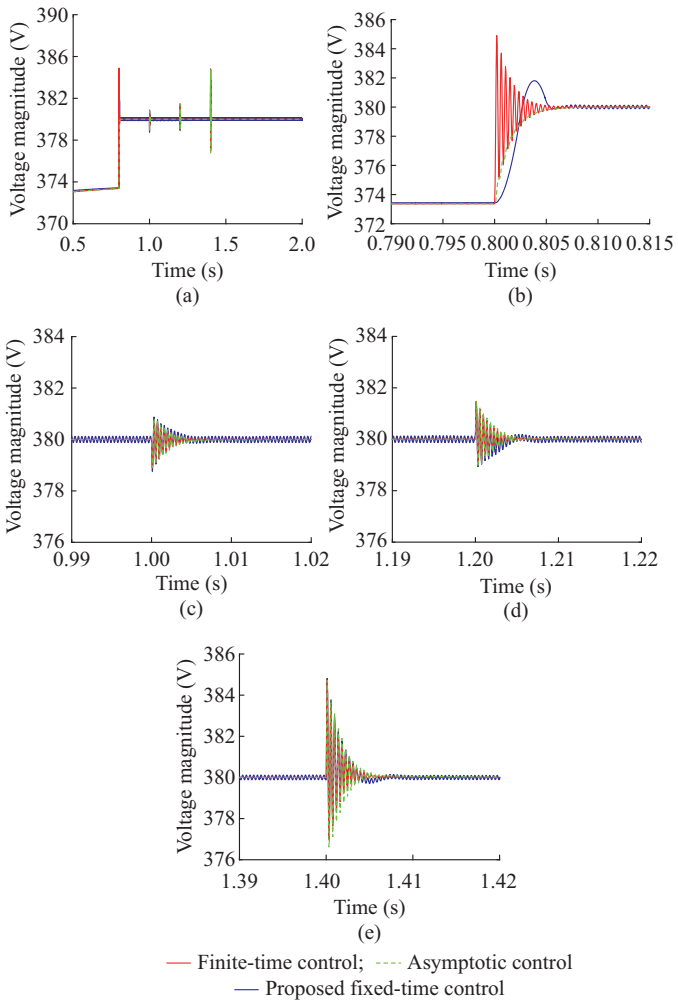

Fig. 6. DG1 output voltage using proposed fixed-time control, finite-time control and asymptotic control. (a) Output voltage. (b) Zoom on time lapse [0.79 s, 0.815 s]. (c) Zoom on time lapse [0.99 s, 1.02 s]. (d) Zoom on time lapse [1.19 s, 1.22 s]. (e) Zoom on time lapse [1.39 s, 1.42 s].

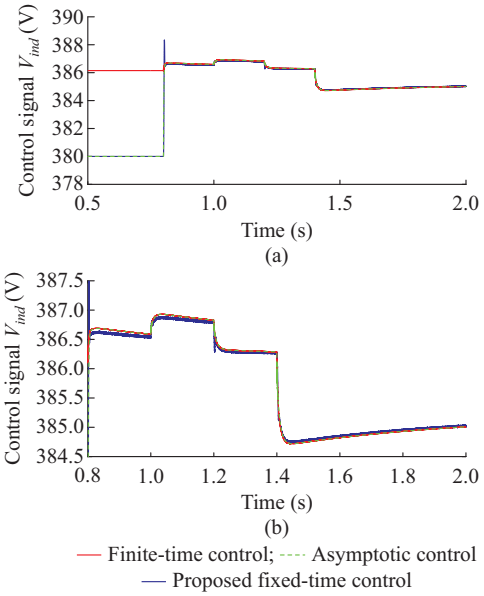

Fig. 7. Control signal V_{ind} of proposed fixed-time controller, finite-time control and asymptotic control. (a) Control signal V_{ind}. (b) Zoom on time lapse [0.8 s, 2 s].

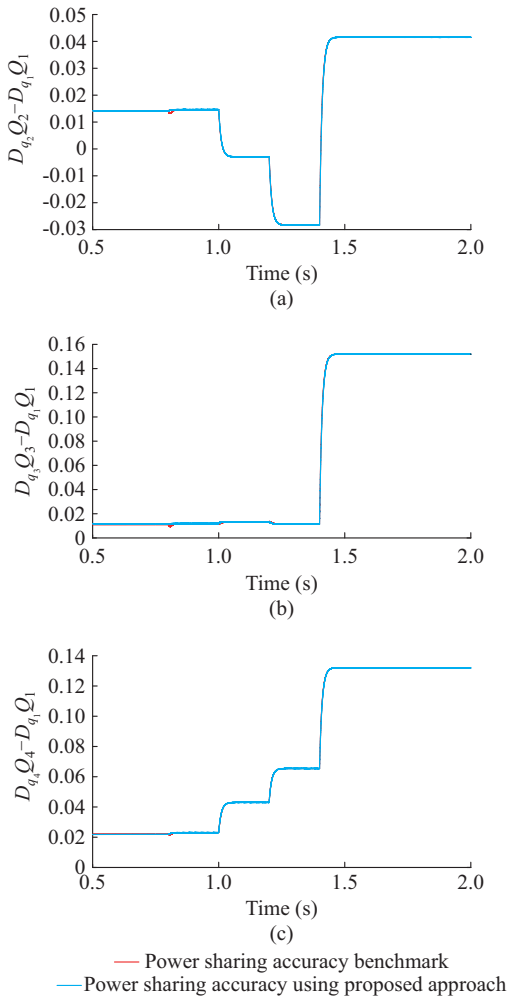

Fig. 8. Error of reactive power sharing using proposed and conventional approaches. (a) $D_{q2}Q_2-D_{q1}Q_1$. (b) $D_{q3}Q_3-D_{q1}Q_1$. (c) $D_{q4}Q_2-D_{q4}Q_1$.

At $t=0.8$ s, the secondary control is activated. Figure 6 shows that the fixed-time secondary control restores the voltage magnitude to its reference before the upper bound of prefixed settling-time of 10 ms with less than 2 V overshoot while maintaining smooth output voltage. However, the finite-time controller provides a fluctuating output voltage with over 12 consecutive overshoots before reaching the reference, which means that the proposed approach enhances the tracking dynamics by 90% compared with that of finite-time control. Unlike the designed fixed-time approach, the asymptotic control also leads to voltage fluctuation during its convergence to the reference. And the reference tracking can not be achieved in a finite time. In the asymptotic control, the reference is only a limit of DG terminal voltage when time goes to infinity. In practical, this means that the reference tracking error can not be canceled using asymptotic control protocols, while the proposed fixed-time control ensures voltage reference tracking before a prefixed maximum settling time despite the external disturbances. For example, the reaching time of the reference is guaranteed to be finite and fixed in advance. In this paper, the fixed-time approach provides 100% better performance than asymptotic approaches on both transient dynamics and steady-state basis.

The primary reactive power control represents the benchmark for power sharing accuracy, i.e., the nominal level to be maintained within the microgrid. The proposed fixed-time secondary control achieves efficient voltage reference tracking while maintaining 100% of power sharing accuracy.

Load power variations begin at $t=1$ s as shown in Figs. 4 and 5. Figure 6 shows that by using fixed-time, finite-time and asymptotic controllers, similar voltage fluctuations occur. Unlike other approaches, the proposed controller rejects the voltage fluctuations before the upper bound of prefixed settling-time of 10 ms, which achieves accurate reactive power sharing.

The control signals displayed in Fig. 7 show that the proposed control system provides better performance with smaller control signal than finite-time and asymptotic approaches. The proposed system has faster dynamics and a smaller steady-state value, which justifies the voltage regulation and reference tracking speed of the proposed approach.

Figure 8 shows that the proposed reactive power controller maintains power sharing accuracy at its benchmark level in presence of load power variations. The voltage control has not been conducted at the expense of reactive power control. Therefore, the proposed power controller have successfully provided better voltage regulation and reference tracking performance while maintaining reactive power sharing accuracy at its nominal level.

V. Conclusion

In this paper, a fixed-time distributed voltage and reactive power secondary control approach for islanded AC microgrids has been designed. The proposed distributed sliding-mode controller ensures voltage regulation and reference tracking before the upper bound of prefixed settling-time despite the unknown disturbances. And accurate reactive power sharing among DGs is maintained. The comparative simulation conducted with load power variations confirms the performance of the controller in voltage regulation and reference tracking before the desired fixed-time, and the accuracy of reactive power sharing is maintained. Simulation results show that the proposed fixed-time control provides better performance in term of voltage regulation and reference tracking than finite-time and asymptotic approaches, which can achieve fast regulation reference tracking at the expense of the system stability with severe voltage fluctuations.

References

[1] X. Lu, X. Yu, J. Lai *et al*., "A novel distributed secondary coordination control approach for islanded microgrids," *IEEE Transactions on Smart Grid*, vol. 9, no. 4, pp. 2726-2740, Jul. 2018.

[2] X. Wu, C. Shen, and R. Iravani, "A distributed, cooperative frequency and voltage control for microgrids," *IEEE Transactions on Smart Grid*, vol. 9, no. 4, pp. 2764-2776, Jul. 2018.

[3] N. M. Dehkordi, N. Sadati, and M. Hamzeh, "Distributed robust finite-time secondary voltage and frequency control of islanded microgrids," *IEEE Transactions on Power Systems*, vol. 32, no. 5, pp. 3648-3659, Sept. 2017.

[4] X. Wang, H. Zhang, and C. Li, "Distributed finite-time cooperative control of droop-controlled microgrids under switching topology," *IET Renewable Power Generation*, vol. 11, no. 5, pp. 707-714, Feb. 2017.

[5] A. Bidram, V. Nasirian, A. Davoudi *et al*., *Cooperative Synchronization in Distributed Microgrid Control*. Heidelberg: Springer Interna-

tional Publishing, 2017.
[6] N. M. Dehkordi, N. Sadati, and M. Hamzeh, "Fully distributed cooperative secondary frequency and voltage control of islanded microgrids," *IEEE Transactions on Energy Conversion*, vol. 32, no. 2, pp. 675-685, Jun. 2017.
[7] J. Schiffer, T. Seel, J. Raisch *et al*., "Voltage stability and reactive power sharing in inverter-based microgrids with consensus-based distributed voltage control," *IEEE Transactions on Control Systems Technology*, vol. 24, no. 1, pp. 96-109, Jan. 2016.
[8] V. Nasirian, S. Moayedi, A. Davoudi *et al*., "Distributed cooperative control of DC microgrids," *IEEE Transactions on Power Electronics*, vol. 30, no. 4, pp. 2288-2303, Apr. 2015.
[9] J. W. Simpson-Porco, Q. Shafiee, F. Dörfler *et al*., "Secondary frequency and voltage control of islanded microgrids via distributed averaging," *IEEE Transactions on Industrial Electronics*, vol. 62, no. 11, pp. 7025-7038, Nov. 2015.
[10] A. Bidram, A. Davoudi, and F. L. Lewis, "A multiobjective distributed control framework for islanded AC microgrids," *IEEE Transactions on Industrial Informatics*, vol. 10, no. 3, pp. 1785-1798, Aug. 2014.
[11] A. Bidram, A. Davoudi, F. L. Lewis *et al*., "Distributed cooperative secondary control of microgrids using feedback linearization," *IEEE Transactions on Power Systems*, vol. 28, no. 3, pp. 3462-3470, Aug. 2013.
[12] H. Cai, G. Hu, F. L. Lewis *et al*., "A distributed feedforward approach to cooperative control of AC microgrids," *IEEE Transactions on Power Systems*, vol. 31, no. 5, pp. 4057-4067, Sept. 2016.
[13] A. Bidram, A. Davoudi, F. L. Lewis *et al*., "Distributed adaptive voltage control of inverter-based microgrids," *IEEE Transactions on Energy Conversion*, vol. 29, no. 4, pp. 862-872, Dec. 2014.
[14] G. Lou, W. Gu, W. Sheng *et al*., "Distributed model predictive secondary voltage control of islanded microgrids with feedback linearization," *IEEE Access*, vol. 6, pp. 50169-50178, Jan. 2018.
[15] G. Lou, W. Gu, Y. Xu *et al*., "Distributed MPC-based secondary voltage control scheme for autonomous droop-controlled microgrids," *IEEE Transactions on Sustainable Energy*, vol. 8, no. 2, pp. 792-804, Apr. 2017.
[16] R. R. Nair, H. Karki, A. Shukla *et al*., "Faulttolerant formation control of nonholonomic robots using fast adaptive gain nonsingular terminal sliding mode control," *IEEE Systems Journal*, vol. 13, no. 1, pp. 1006-1017, Mar. 2019.
[17] M. Van, M. Mavrovouniotis, and S. Ge, "An adaptive backstepping nonsingular fast terminal sliding mode control for robust fault tolerant control of robot manipulators," *IEEE Transactions on Systems, Man, and Cybernetics: Systems*, vol. 49, no. 7, pp. 1448-1458, Jul. 2019.
[18] H. Wang, Y. Pan, S. Li *et al*., "Robust sliding mode control for robots driven by compliant actuators," *IEEE Transactions on Control Systems Technology*, vol. 27, no. 3, pp. 1259-1266, May 2019.
[19] A. Ferrara and G. P. Incremona, "Design of an integral suboptimal second-order sliding mode controller for the robust motion control of robot manipulators," *IEEE Transactions on Control Systems Technology*, vol. 23, no. 6, pp. 2316-2325, Nov. 2015.
[20] Q. Yang, M. Saeedifard, and M. A. Perez, "Sliding mode control of the modular multilevel converter," *IEEE Transactions on Industrial Electronics*, vol. 66, no. 2, pp. 887-897, Feb. 2019.
[21] J. Liu, Y. Yin, W. Luo *et al*., "Sliding mode control of a three-phase AC/DC voltage source converter under unknown load conditions: industry applications," *IEEE Transactions on Systems, Man, and Cybernetics: Systems*, vol. 48, no. 10, pp. 1771-1780, Oct. 2018.
[22] W. Qi, S. Li, S Tan *et al*., "Parabolic-modulated slidingmode voltage control of a buck converter," *IEEE Transactions on Industrial Electronics*, vol. 65, no. 1, pp. 844-854, Jan. 2018.
[23] R. Ling, D. Maksimovic, and R. Leyva, "Second-order sliding-mode controlled synchronous buck DC-DC converter," *IEEE Transactions on Power Electronics*, vol. 31, no. 3, pp. 2539-2549, Mar. 2016.
[24] Q. Wang, H. Yu, M. Wang *et al*., "An improved sliding mode control using disturbance torque observer for permanent magnet synchronous motor," *IEEE Access*, vol. 7, pp. 36691-36701, Feb. 2019.
[25] M. A. M. Cheema, J. E. Fletcher, M. Farshadnia *et al*., "Sliding mode based combined speed and direct thrust force control of linear permanent magnet synchronous motors with first-order plus integral sliding condition," *IEEE Transactions on Power Electronics*, vol. 34, no. 3, pp. 2526-2538, Mar. 2019.
[26] X. Wang, M. Reitz, and E. E. Yaz, "Field oriented sliding mode control of surface-mounted permanent magnet ac motors: theory and applications to electrified vehicles," *IEEE Transactions on Vehicular Technology*, vol. 67, no. 11, pp. 10343-10356, Nov. 2018.
[27] M. A. M. Cheema, J. E. Fletcher, M. Farshadnia *et al*., "Combined speed and direct thrust force control of linear permanent-magnet synchronous motors with sensorless speed estimation using a sliding-mode control with integral action," *IEEE Transactions on Industrial Electronics*, vol. 64, no. 5, pp. 3489-3501, May 2017.
[28] R. Zhang and B. Hredzak, "Nonlinear sliding mode and distributed control of battery energy storage and photovoltaic systems in AC microgrids with communication delays," *IEEE Transactions on Industrial Informatics*, vol. 15, no. 9, pp. 5149-5160, Sept. 2019.
[29] Y. Huang, Z. Zhang, W. Huang *et al*., "DC-link voltage regulation for wind power system by complementary sliding mode control," *IEEE Access*, vol. 7, pp. 22773-22780, Feb. 2019.
[30] I. Villanueva, A. Rosales, P. Ponce *et al*., "Grid voltage oriented sliding mode control for DFIG under balanced and unbalanced grid faults," *IEEE Transactions on Sustainable Energy*, vol. 9, no. 3, pp. 1090-1098, Jul. 2018.
[31] A. Merabet, L. Labib, A. M. Y. M. Ghias *et al*., "Robust feedback linearizing control with sliding mode compensation for a grid-connected photovoltaic inverter system under unbalanced grid voltages," *IEEE Journal of Photovoltaic*s, vol. 7, no. 3, pp. 828-838, May 2017.
[32] R. Guzman, L. G. de Vicuna, J. Morales *et al*., "Sliding-mode control for a three-phase unity power factor rectifier operating at fixed switching frequency," *IEEE Transactions on Power Electronics*, vol. 31, no. 1, pp. 758-769, Jan. 2016.
[33] S. Y. Gadelovits, D. Insepov, V. Kadirkamanathan *et al*., "Uncertainty and disturbance estimator based controller equipped with a multiple-time-delayed filter to improve the voltage quality of inverters," *IEEE Transactions on Industrial Electronics*, vol. 66, no. 11, pp. 8947-8957, Nov. 2019.
[34] M. Ghanaatian and S. Lotfifard, "Control of flywheel energy storage systems in the presence of uncertainties," *IEEE Transactions on Sustainable Energy*, vol. 10, no. 1, pp. 36-45, Jan. 2019.
[35] P. M. Shabestari, S. Ziaeinejad, and A. Mehrizi-Sani, "Reachability analysis for a grid-connected voltage-sourced converter (VSC)," in *Proceedings of 2018 IEEE Applied Power Electronics Conference and Exposition (APEC)*, San Antonio, USA, Mar. 2018, pp. 2349-2354.
[36] F. Liu, Y. Li, Y. Cao *et al*., "A two-layer active disturbance rejection controller design for load frequency control of interconnected power system," *IEEE Transactions on Power Systems*, vol. 31, no. 4, pp. 3320-3321, Jul. 2016.
[37] F. Farzan, M. A. Jafari, R. Masiello *et al*., "Toward optimal day-ahead scheduling and operation control of microgrids under uncertainty," *IEEE Transactions on Smart Grid*, vol. 6, no. 2, pp. 499-507, Mar. 2015.
[38] M. Ghazzali, M. Haloua, and F. Giri, "Modeling and adaptive control and power sharing in islanded AC microgrids," *International Journal of Control Automation and Systems*, vol. 18, no. 5, pp. 1229-1241, May 2020.
[39] N. Pogaku, M. Prodanovic, and T. C. Green, "Modeling, analysis and testing of autonomous operation of an inverter-based microgrid," *IEEE Transactions on Power Electronics*, vol. 22, no. 2, pp. 613-625, Mar. 2007.
[40] M. S. Sadabadi, Q. Shafiee, and A. Karimi, "Plug-and-play voltage stabilization in inverter-interfaced microgrids via a robust control strategy," *IEEE Transactions on Control Systems Technology*, vol. 25, no. 3, pp. 781-791, May 2017.
[41] W. Leonhard, *Control of Electrical Drives*. Heidelberg: Springer-Verlag, 2001.
[42] A. Khanzadeh and M. Pourgholi, "Fixed-time leader-follower consensus tracking of second-order multi-agent systems with bounded input uncertainties using non-singular terminal sliding mode technique," *IET Control Theory Applications*, vol. 12, no. 5, pp. 679-686, Jan. 2018.
[43] C. Moldovan, C. Damian, and O. Georgescu, "Voltage level increase in low voltage networks through reactive power compensation using capacitors," *Procedia Engineering*, vol. 181, pp. 731-737, Jan. 2017.

Mohamed Ghazzali received the engineering degree in automation and industrial computer science from Mohammadia School of Engineers, University Mohammed V, Rabat, Morocco, in 2017. He is currently pursuing the Ph.D. degree with the same school. His current research interests include cooperative control, distributed control and power optimization of microgrids.

Mohamed Haloua received the D.E.S. and the Ph.D. degrees in automatic control from the University Mohammed V, Rabat, Morocco, in 1987 and 1993, respectively. He is currently a Professor of control engineering at the Department of Electrical Engineering, Ecole Mohammadia d'Ingenieurs, Rabat, Morocco. His research interests include system identification, nonlinear

and robust control and their applications.

Fouad Giri received the Ph.D. degree in automatic control from Institut National Polytechnique de Grenoble, Grenoble, France, in 1988. He is currently a Professor at the University de Caen Normandie, Caen, France. His research interests include nonlinear system identification, observation and control, and application to power electric systems.